Numerical Study of Wave Propagation in a Non-uniform Flow

Alex Povitsky
ICASE, Hampton, Virginia

The NASA STI Program Office . . . in Profile

Since its founding, NASA has been dedicated to the advancement of aeronautics and space science. The NASA Scientific and Technical Information (STI) Program Office plays a key part in helping NASA maintain this important role.

The NASA STI Program Office is operated by Langley Research Center, the lead center for NASA's scientific and technical information. The NASA STI Program Office provides access to the NASA STI Database, the largest collection of aeronautical and space science STI in the world. The Program Office is also NASA's institutional mechanism for disseminating the results of its research and development activities. These results are published by NASA in the NASA STI Report Series, which includes the following report types:

- TECHNICAL PUBLICATION. Reports of completed research or a major significant phase of research that present the results of NASA programs and include extensive data or theoretical analysis. Includes compilations of significant scientific and technical data and information deemed to be of continuing reference value. NASA counter-part or peer-reviewed formal professional papers, but having less stringent limitations on manuscript length and extent of graphic presentations.

- TECHNICAL MEMORANDUM. Scientific and technical findings that are preliminary or of specialized interest, e.g., quick release reports, working papers, and bibliographies that contain minimal annotation. Does not contain extensive analysis.

- CONTRACTOR REPORT. Scientific and technical findings by NASA-sponsored contractors and grantees.

- CONFERENCE PUBLICATIONS. Collected papers from scientific and technical conferences, symposia, seminars, or other meetings sponsored or co-sponsored by NASA.

- SPECIAL PUBLICATION. Scientific, technical, or historical information from NASA programs, projects, and missions, often concerned with subjects having substantial public interest.

- TECHNICAL TRANSLATION. English-language translations of foreign scientific and technical material pertinent to NASA's mission.

Specialized services that help round out the STI Program Office's diverse offerings include creating custom thesauri, building customized databases, organizing and publishing research results . . . even providing videos.

For more information about the NASA STI Program Office, you can:

- Access the NASA STI Program Home Page at http://www.sti.nasa.gov/STI-homepage.html

- Email your question via the Internet to help@sti.nasa.gov

- Fax your question to the NASA Access Help Desk at (301) 621-0134

- Phone the NASA Access Help Desk at (301) 621-0390

- Write to:
  NASA Access Help Desk
  NASA Center for AeroSpace Information
  7121 Standard Drive
  Hanover, MD 21076-1320

NASA/CR-2000-210533
ICASE Report No. 2000-35

Numerical Study of Wave Propagation in a Non-uniform Flow

Alex Povitsky
ICASE, Hampton, Virginia

Institute for Computer Applications in Science and Engineering
NASA Langley Research Center
Hampton, VA

Operated by Universities Space Research Association

National Aeronautics and
Space Administration

September 2000

NUMERICAL STUDY OF WAVE PROPAGATION IN A NON-UNIFORM FLOW

ALEX POVITSKY*

Abstract. The propagation of acoustic waves originating from cylindrical and spherical pulses, in a non-uniform mean flow, and in the presence of a reflecting wall is investigated by Hardin and Pope approach using compact approximation of spatial derivatives. The 2-D and 3-D stagnation flows and a flow around a cylinder are taken as prototypes of real world flows with strong gradients of mean pressure and velocity. The intensity and directivity of acoustic wave patterns appear to be quite different from the benchmark solutions obtained in a static environment for the same geometry. The physical reasons for amplification and weakening of sound are discussed in terms of dynamics of wave profile and redistribution of acoustic energy and its potential and kinetic components. For an acoustic wave in the flow around a cylinder, the observed mean acoustic pressure is approximately doubled (upstream pulse position) and halved (downstream pulse position) in comparison with the sound propagation in static ambient conditions.

Key words. aeroacoustics, non-uniform mean flow, higher-order compact scheme, amplification of sound, stagnation flow, flow around cylinder

Subject classification. Fluid Mechanics

1. Introduction. This study investigates numerically the influence of strong mean flow gradients on the directivity and strength of sound waves propagating in such a flow.

The goal of this study is to get computational insight into physical mechanisms of angular redistribution of acoustic energy and acoustic pressure. The considered mean flows include potential flow around a circular cylinder, the 2-D and 3-D stagnation flows, and a 90° corner flow. These idealized mean flows mimic real world flows in areas of strong sound reflection and generation such as a leading edge of a wing or a turbine blade, a protruding corner of a wall cavity, a wing-fuselage intersection, an impingement area of a jet, and a flow behind a bluff body.

The amplification or weakening of sound propagating in non-uniform flows has attracted considerable attention of researchers. However, available computational studies are mainly restricted to one-dimensional mean flows.

For one-dimensional flow in a duct with variable cross-section, the acoustic pressure appears to concentrate towards the duct centerline or the duct wall for upstream and downstream sound propagation, respectively [11], [15]. Motivated by engine noise, the authors of these studies use the wave envelope method (WEM) to study propagation of sound in one-dimensional and quasi one-dimensional mean flows This method is based on consideration of the governing acoustic variables as sums of harmonics. Additional assumptions are made about rapid axial oscillations and slowly varying amplitude and phase corrections caused by the non-uniformity of the flow.

Atassi and Grzedzinsky [2] considered propagation of unsteady disturbances in flows around bodies with a stagnation point. For incompressible mean flows, the aeroacoustic problem is formulated in terms of an integral equation of the Fredholm type. The considered streamlined body and the corresponding

---

potential mean flow result from superposition of a uniform flow and a source. Yet, additional assumptions and simplifications (some of them depend on the type of potential background flow) are needed to perform integration. Authors [2] present the disturbance pressure along the stagnation streamline that shows increase of the disturbance pressure for an upstream harmonic disturbance.

Hardin and Pope approach [7] implies consideration of a flowfield as a sum of the mean velocity and a disturbance field and solution of disturbance variables in time and space domain by explicit integration in time and use of appropriate spatial discretization. The computational methodology used in the current study is based on above approach.

In order to use an analytical solution for mean flow, the flow in the current study is assumed to be potential, i.e., inviscid and incompressible. The speed of sound (relative to the local mean flow velocity) is assumed to be equal to unity. These assumptions are fair unless the Mach number exceeds 0.5.

In this paper, the relative orientation of the direction of wave propagation, mean pressure gradient, and the mean flow vector are studied to show the amplification or weakening of the acoustic pressure. The consideration starts with two-dimensional stagnation mean flows, then the approach is expanded to three-dimensional stagnation mean flows, and, finally, applied to the inviscid flow around circular cylinder.

In all considered cases, the obtained acoustic pressure is compared with that for the wave propagation under static ambient conditions and for the same geometry of surrounding rigid boundaries.

Variation of directivity of acoustic pressure implies changes in directivity of acoustic energy in comparison with the sound propagation under static ambient conditions. This paper studies angular redistribution of acoustic energy and its potential and kinetic components in non-uniform mean flows. The acoustic energy is a sum of potential and kinetic components where the potential energy is closely related to the averaged-in-time root mean square of acoustic pressure which is usually measured by experimentalists as an indicator of noise intensity.

Our recent study [12] shows that the generation of sound waves originated from entropy sources is caused by baroclinic generation of disturbance vorticity as a result of interaction of the mean flow pressure gradient and the wave density gradient. In turn, this generated vorticity causes the generation (or sink) of acoustic energy by the source term in the acoustic energy equation. Order of magnitude analysis suggests that the source term can not be neglected in the acoustic energy equation. This study presents vorticity and energy source terms obtained from numerical simulation. For the propagation of acoustic waves originated from an acoustic pulse (as opposed to the sound generation from entropy or vorticity pulses [12]), The major effect of the non-uniformity of the mean flow on the wave propagation (as opposed to the wave generation from entropy or vorticity pulses [12]) is the angular redistribution of acoustic energy and kinetic-to-potential transform whereas the newly generated acoustic energy appears to be minor.

The article is built as follows. In Section 2, the wave propagation originated from a cylindrical 2-D source in 2-D stagnation-type flows is studied and numerical results about amplification of acoustic pressure, alternation of wave pattern, and acoustic energy redistribution are presented. In Section 3, the wave propagation from a spherical source is considered in 3-D stagnation flows. The symmetric 3-D stagnation flow with a single stagnation point and the 3-D stagnation flow with stagnation line flow are taken as typical representatives of three-dimensional stagnation mean flows. In Section 4, the inviscid flow around a circular cylinder is considered for various subsonic Mach numbers of the mean flow. Amplification of sound (for upstream wave propagation) and weakening of sound (for downstream wave propagation) is studied in this Section.

2. Sound propagation in a 2-D stagnation-type mean flow. The common type of mean flow is that the flux across a given surface is equal to zero, either because the surface is a symmetry surface or because the surface is the boundary of a rigid body [3]. If two straight zero-flux boundaries intersecting at an angle π/n the stream-function field for incompressible flow is given by

$$\psi = A r^n sin(n\theta), \tag{2.1}$$

where (r, θ) are polar coordinates. Note that $\psi = 0$, if $\theta = 0$ or $\theta = \pi/n$. For example, the 2-D stagnation flow

$$U = x, \; V = -y \tag{2.2}$$

is a union of two flows with $n = 2$ where the dividing streamline is the symmetry axis of the flow.

Introducing a disturbance, instantaneous velocities and density are considered as sums of the known steady incompressible mean flow (see above) and the unsteady compressible isentropic disturbance

$$u = U + u\prime, v = V + v\prime, p = P + p\prime, \rho = 1 + \rho\prime. \tag{2.3}$$

The normalized speed of sound is assumed to be equal to unity and, therefore, pressure and density disturbances are equal for acoustic pulse. Substituting above sums to the Euler equations, the dynamic equations for unsteady (disturbance) components of mass and momentum fluxes are obtained

$$\boldsymbol{q}_t + \boldsymbol{f}_x + \boldsymbol{g}_y = 0, \tag{2.4}$$

where

$$\boldsymbol{q} = \begin{pmatrix} \rho\prime \\ (1+\rho\prime)(U+u\prime) \\ (1+\rho\prime)(V+v\prime) \end{pmatrix}, \; \boldsymbol{f} = \begin{pmatrix} (1+\rho\prime)(U+u\prime) \\ (1+\rho\prime)(U+u\prime)^2 + (P+p\prime) \\ (1+\rho\prime)(U+u\prime)(V+v\prime) \end{pmatrix}, \; \boldsymbol{g} = \begin{pmatrix} (1+\rho\prime)(V+v\prime) \\ (1+\rho\prime)(U+u\prime)(V+v\prime) \\ (1+\rho\prime)(V+v\prime)^2 + (P+p\prime) \end{pmatrix}.$$

$$\tag{2.5}$$

The equations are linearized and solved with respect to unknown disturbance variables in space-time domain

$$\frac{\partial u}{\partial t} = -\frac{\partial p}{\partial x} - U\frac{\partial u}{\partial x} - \frac{\partial U}{\partial x}u - V\frac{\partial u}{\partial y} - \frac{\partial U}{\partial y}v - V\frac{\partial U}{\partial y}\rho - U\frac{\partial U}{\partial x}\rho,$$

$$\frac{\partial v}{\partial t} = -\frac{\partial p}{\partial y} - V\frac{\partial v}{\partial y} - U\frac{\partial v}{\partial x} - \frac{\partial V}{\partial x}u - \frac{\partial V}{\partial y}v - U\frac{\partial V}{\partial x}\rho, -V\frac{\partial V}{\partial y}\rho,$$

$$\frac{\partial \rho}{\partial t} = -\frac{\partial u}{\partial x} - \frac{\partial v}{\partial y} - U\frac{\partial \rho}{\partial x} - V\frac{\partial \rho}{\partial y}. \tag{2.6}$$

The spatial derivatives of the mean flow variables for arbitrary n are presented in Appendix A. The non-linear set of equations for the 2-D stagnation mean flow is presented in our study [12].

2.1. Numerical algorithm and the code validation. The solution is advanced in time in five sub-stages per time step using a low-storage explicit-in-time fourth-order Runge-Kutta (RK) scheme scheme proposed by Williamson [16] and implemented by Wilson et al. [17].

The spatial derivatives of unknown disturbance variables are approximated using compact finite difference schemes [10] applied to natural variables $u\prime, v\prime$ and $\rho\prime$

$$\alpha U_{i-1}^{'} + U_i^{'} + \alpha U_{i+1}^{'} = \frac{a}{2\Delta x}(U_{i+1} - U_{i-1}) + \frac{b}{2\Delta x}(U_{i+2} - U_{i-2}), \tag{2.7}$$

where U'_{i-1}, U'_i, and U'_{i+1} are unknown derivatives at grid nodes $i-1, i$, and $i+1$, Δx is the grid step and $U_{i-2}, ..., U_{i+2}$ denote values of variable U at grid nodes $i-2, ..., i+2$. The values of U are taken from the previous stage of the RK scheme. Here the classical fourth-order Padé compact scheme ($\alpha = 0.25$, $a = 1.5$ and $b = 0$) which has a tridiagonal matrix for the right and left sides of (2.7) is used.

At all boundaries but a rigid plate characteristic inflow or outflow boundary conditions are applied to disturbance variables. At a rigid surface, reflection boundary conditions are used for pressure disturbance and for the parallel to the surface component of velocity disturbance whereas the normal to the rigid surface component of velocity is taken equal to zero. Discretization of spatial derivatives in the direction perpendicular to a boundary are computed by one-sided finite differences at all boundaries [4].

The system (2.7) with near-boundary one-sided differences is solved by version of Gaussian elimination for narrow banded systems known as the Thomas algorithm [9] applied to each line of numerical grid in all spatial directions.

To validate the code against the known analytical solution [8], the static ambient conditions (i.e., the mean flow velocity is equal to zero) are taken. In this case, the right-hand side of system (2.6) is simplified as follows

$$
\frac{\partial u}{\partial t} = -\frac{\partial p}{\partial x}
$$
$$
\frac{\partial v}{\partial t} = -\frac{\partial p}{\partial y}
$$
$$
\frac{\partial \rho}{\partial t} = -\frac{\partial u}{\partial x} - \frac{\partial v}{\partial y} \tag{2.8}
$$

The initial 2-D cylindrical acoustic pulse is given by

$$
p = \rho = \epsilon \exp\left[-d^2 \frac{(x-x_c)^2 + (y-y_c)^2}{a}\right], \tag{2.9}
$$

where $\epsilon = 0.01, a = ln(2)/9, d = 60$ is the normalization coefficient, (x_c, y_c) is the pulse center coordinates.

To check the symmetry of solution, the computational domain is taken as a union of $[-1, 1] \times [-1, 0]$ and $[-1, 1] \times [0, 1]$ subdomains separated by a rigid flat plate located at $y = 0$. The couple of initial pulses (2.9) is located at $(0, \pm 0.25)$. Isolines of acoustic pressure for this problem at 160×160 grid per subdomain are presented in Fig. 1 at $t = 0.5$. The isobar values are uniformly distributed between the maximum and minimum of acoustic pressure. Although the Thomas algorithm is, strictly speaking, non-symmetric (as any Gaussian elimination), the acoustic pressure field in Fig. 1a is perfectly symmetric.

The results of grid refinement study are presented in Fig. 1b for $[-1, 1] \times [0, 1]$ computational domain covered with $80 \times 80, 120 \times 120$, and 160×160 numerical grids. The visible wiggles exist only for the coarse grid and the solution approaches the analytical solution including most critical points of the maximum and minimum of the reflected wave. For the transmitted wave, the numerical solution practically coincide with the analytical solution [8] for finer grids. Therefore, the grid 160×160 has been adopted in this study.

2.2. Distribution of acoustic pressure. To study the acoustic pressure distribution in a non-uniform flow, the 2-D stagnation inviscid mean flow is taken as an example (Case 2-A). The velocity field of the stagnation mean flow and isobars of the initial acoustic pulse, centered at $(0, 0.25)$, are presented in Fig. 2a (left). The speed of sound is equal to unity and is presented in Fig. 2a for scale. As far as the stagnation flowfield satisfies Eq. (2.2), the Mach number at a point is equal to the local distance from the origin, i.e., the Mach number at the location of the center of initial pulse is equal to 0.25.

4

The propagation of sound is described by the system (2.6) where the mean flow is given by (2.1) with $n = 2$. Grid refinement study for Case 2-A is presented in [12] and shows that the results on the 160×160 and 200×200 grids are quite closed to each other that confirms the use of the former grid for simulations.

The isobars of acoustic pressure are presented in Fig. 2a (right) at $t = 0.5$. Approximate centerline coordinates of the maximums of acoustic pressure for the transmitted and reflected waves are 0.5 and 0.25, respectively. Note that the Mach numbers at these points are equal to their $y-$ coordinate values (see above). As expected, the acoustic isobars obtained in the static ambient conditions, denoted here as Case 2-B, (Fig. 1a) are different from those in the Case 2-A at the same time moment. In the Case 2-A, the $y-$coordinate of the wave front at the neighborhood of the centerline is smaller and the $x-$coordinate of the wave front near the wall is larger than those in the Case 2-B. The explanation is straightforward and is based on the fact that the speed of sound in a steady frame is equal to $c + U$, where c is the local speed of sound and U is the local velocity of the flowfield.

The density of isobars is larger at the neighborhood of the centerline and smaller near the wall in the Case 2-A in comparison with those in the Case 2-B. In Fig. 3a, the acoustic pressure profiles at the centerline are presented for both cases at $t = 0.5$. The maximum absolute value of acoustic pressure is approximately 80% larger for the transmitted wave and two times larger for the reflected wave than those in the Case 2-B. Recall, that the speed of wave propagation is $c + U$. While the wave propagates upstream the decelerating subsonic flow, its front moves slower than its back. The situation is opposite for the accelerating flow (which is the case near the wall). Thus, the wave front becomes narrower at the neighborhood of the centerline and wider while the stagnation flow spread along the wall in comparison to those in static ambient conditions.

Accelerating mean flow (backward 2-D stagnation flow) is considered to study the influence of the mean flow direction on the wave patterns (Fig. 2b). The initial position of acoustic pulse, the mean flow streamlines and the mean pressure distribution remain the same as for the Case 2-A. (compare Fig. 2b with Fig. 2a). However, the direction of the maximum acoustic pressure has been considerably changed from being perpendicular to the wall to being parallel to it. Still, the maximum acoustic pressure corresponds to the direction where the sound propagates upstream of the mean flow.

To study the influence of the background flow while the acoustic pulse is located off the centerline and two reflecting surfaces are present, the 90°- corner geometry is considered (Fig. 7). The rigid plains coincide with the Cartesian axis. The potential flow in this geometry is described by a single stagnation flow with $n = 2$ flowing to the right. Initial position of acoustic pulse is taken $(0.25, 0.25)$, where the local Mach number of the mean flow is approximately equal to 0.35.

Computational results in terms of acoustic pressure are compared with those obtained in the Case 2-B. In the latter case the maximum acoustic pressure is in the bisector direction and the cylindrical shape of wave pattern is symmetric with respect to the bisector (Fig. 7b). In presence of the mean flow, the waves flatten, especially in the neighborhood of the $y-$axis, where the sound propagates upstream of the mean flow (Fig. 7a). The maximum acoustic pressure increases about 40% in comparison with that in the static ambient conditions.

2.3. Distribution of acoustic energy. To get physical insight into amplification of acoustic pressure, acoustic energy is considered here. Transport equation of acoustic energy density for irrotational and incompressible mean flow and adiabatic acoustic disturbance is given by [6]:

$$\frac{\partial E}{\partial t} + \nabla \boldsymbol{I} = \boldsymbol{u\prime} \cdot (\boldsymbol{U} \times \boldsymbol{\omega\prime}), \tag{2.10}$$

where

$$E = p\prime^2/2 + u\prime^2/2 + \rho\prime u\prime \cdot U \tag{2.11}$$

is the acoustic energy density and

$$I = (p\prime + u\prime \cdot U)(u\prime + \rho\prime U) \tag{2.12}$$

is the acoustic energy flux.

The acoustic energy is a sum of potential energy $Pot = p\prime^2/2$, that mimics the strength of acoustic pressure in compressible media, and kinetic energy $K = u\prime^2/2 + \rho\prime u\prime \cdot U$.

The centerline distribution of E is presented in Fig. 3b, where the curve 1 corresponds to the Case 2-A and the curve 2 corresponds to the Case 2-B. For the reflected wave, the local maximum of E in the Case 2-A is about three times greater than that in the Case 2-B. Its location is the same as that for the maximum acoustic pressure (compare Fig. 3b to Fig. 3a) and the ratio of acoustic energies is similar to the ratio of squares of acoustic pressures (four times). It is not the case for the transmitted wave, where the maximum values of E are almost the same in cases 2-A and 2-B in spite of the obvious difference in the acoustic pressure values.

To show the total acoustic energy along the centerline, the integrals

$$I_E = \int_0^y E(y)dy \tag{2.13}$$

and

$$I_P = \int_0^y Pot(y)dy \tag{2.14}$$

are plotted as functions of y at the time moment $t = 0.5$ in Fig. 3c. Obviously, the integrals reach their maximum when the coordinate y exceeds the front coordinate of the transmitted wave. The values of these maximums for integral of acoustic energy differ only by 15% whereas the difference in integrals of potential energy is about two times. Thus, the amplification of sound along the centerline occurs mainly by increase of the potential part in total acoustic energy.

On the contrary, for the bisector direction (45°) and for a near-wall direction (75°) the part of potential energy remains approximately the same for the stagnation mean flow and for the static ambient conditions. Therefore, the weakening of sound near the wall occurs mainly due to the angular redistribution of acoustic energy. The direction-dependent behavior of acoustic energy is explained by the relative value of the last term in (2.11). If sound propagates upstream of the mean flow, the vectors in the inner product $u\prime \cdot U$ are collinear, therefore, the variation of U in a non-uniform mean flow leads to more prominent reduction of the kinetic energy in comparison with other directions. The kinetic energy transforms into potential energy and leads to increase of potential part in the acoustic energy.

To study the generation of acoustic energy by means of interaction of the wave with the non-uniform mean flow, we present here the simplified form of the vorticity transport equation [12]:

$$\frac{D\omega\prime}{Dt} = \nabla\rho\prime \times \nabla P. \tag{2.15}$$

Note that the presence of the pressure gradient in the mean flow (i.e., non-uniformity of the flow) leads to non-zero right-hand side of above equation. Otherwise, the vorticity $\omega\prime$ remains equal to zero as in an irrotational mean flow. In turn, the non-zero $\omega\prime$ leads to the non-zero source term in the energy equation

(2.10). The vorticity is generated where the acoustic wave passes, i.e. $\nabla \rho\prime \neq 0$. As far as $u\prime$ is a multiplier in the right-hand side of Eq. (2.10), the exchange of energy between the steady mean flow and the unsteady disturbance occurs only in presence of the wave. The generated vorticity flows with the local speed of background flow and eventually the vorticity is left behind the wave, that moves with the sonic speed. The instantaneous pattern of the vorticity generation source and the acoustic energy source at $t = 0.5$ are shown in Fig. 5. As expected, areas of maximum acoustic energy generation coincide with instantaneous positions of the reflected and transmitted waves.

Approximately, the maximum value of the energy source term is located at the bisector direction (45^0). In Fig. 6, the acoustic energy and its source are shown as functions of the distance from the origin along the bisector line at $t = 0.5$. The maximum value of the source is approximately one order of magnitude smaller than that for the acoustic energy. Therefore, the local gain of acoustic energy is small in comparison with the angular redistribution of acoustic energy and kinetic-to-potential transforms considered above.

3. Acoustic pulse in the 3-D stagnation flow. In this section we consider a spherical pulse propagating in a 3-D stagnation flow. The 3-D stagnation flow with a single stagnation point at the origin is denoted as Case 3-A and given by

$$W = -z, \ U = 0.5x, \ V = 0.5y. \tag{3.1}$$

The stagnation flow with the stagnation line (Case 3-B) is

$$W = -z, \ U = x, \ V = 0. \tag{3.2}$$

The developed code is readily available for 3-D parallel computations as well [13].

In Case 3-A, the propagation of disturbance is described by the following system of equations

$$\frac{\partial u}{\partial t} = -\frac{\partial p}{\partial x} + 0.5(-x\frac{\partial u}{\partial x} - u - y\frac{\partial u}{\partial y} - x\rho) + z\frac{\partial u}{\partial z}$$

$$\frac{\partial v}{\partial t} = -\frac{\partial p}{\partial y} + 0.5(-y\frac{\partial v}{\partial y} - x\frac{\partial v}{\partial x} - v - y\rho) + z\frac{\partial v}{\partial z},$$

$$\frac{\partial w}{\partial t} = -\frac{\partial p}{\partial z} + 0.5(-y\frac{\partial w}{\partial y} - x\frac{\partial w}{\partial x}) + w - z\rho + z\frac{\partial w}{\partial z},$$

$$\frac{\partial \rho}{\partial t} = -\frac{\partial u}{\partial x} - \frac{\partial v}{\partial y} - \frac{\partial w}{\partial z} + 0.5(-x\frac{\partial \rho}{\partial x} - y\frac{\partial \rho}{\partial y}) + z\frac{\partial \rho}{\partial z}. \tag{3.3}$$

In Case 3-B, the governing system of equations is given by

$$\frac{\partial u}{\partial t} = -\frac{\partial p}{\partial x} - x\frac{\partial u}{\partial x} - u - x\rho + z\frac{\partial u}{\partial z}$$

$$\frac{\partial v}{\partial t} = -\frac{\partial p}{\partial y} - x\frac{\partial v}{\partial x} + z\frac{\partial v}{\partial z},$$

$$\frac{\partial w}{\partial t} = -\frac{\partial p}{\partial z} - x\frac{\partial w}{\partial x} + w - z\rho + z\frac{\partial w}{\partial z},$$

$$\frac{\partial \rho}{\partial t} = -\frac{\partial u}{\partial x} - \frac{\partial v}{\partial y} - \frac{\partial w}{\partial z} - x\frac{\partial \rho}{\partial x} + z\frac{\partial \rho}{\partial z}. \tag{3.4}$$

The initial 3-D spherical acoustic pulse is given by an expression similar to (2.9).

To validate the code, the computations are performed on a set of numerical grids where the wave spreads under static ambient conditions and in presence of the rigid reflecting plate (Case 3-C). The analytic solution for acoustic pressure in case of the infinite domain is given by

$$p = \frac{\epsilon}{2r}\{(r - t)\exp[-a(r - t)^2] + (r + t)\exp[-a(r + t)^2]\}, \tag{3.5}$$

where r is the location of the pulse center at $t = 0$. Solution for the semi-infinite domain is obtained by use of the image pulse located at $-r$:

$$p = p(r) + p(-r). \tag{3.6}$$

Results of computations on 80^3, 120^3, and 160^3 grids are compared to the above analytic solution. Profiles of the centerline acoustic pressure on the above set of grids at $t = 0.5$ are presented in Fig. 8. The observations from the grid refinement study are similar to those obtained for the 2-D case (Section 2). The numerical solution on the 160^3 numerical grid practically coincides with the analytic solution and this grid is used for numerical simulations.

To compare acoustic fields in Cases 3-A, 3-B, and 3-C, the isolines of acoustic pressure at $t = 0.5$ are shown in Fig. 9. In Cases 3-A and 3-C (Fig. 9a, b), the acoustic field is uniform with respect to the direction in the $x - y$ plane. The presence of the stagnation flow leads to amplification of sound at the neighborhood of the centerline. In Case 3-B, the wave pattern is direction-dependent: the maximum elongation of the wave pattern along the rigid plane occurs in the section $x - z$, whereas the minimum elongation is in the section $y - z$. In the latter case, the elongation is closed to that for the Case 3-C (compare Fig. 9a to Fig. 9d). Yet, the centerline position of the pulse is the same in Cases 3-A and 3-B (see Fig. 9b,c, and d).

The centerline acoustic pressure for Cases 3-A and 3-B is presented together with its counterpart for the Case 3-C at $t = 0.5$ in Fig. 10. In spite of the different wave pattern in Cases 3-A and 3-B, the centerline profiles coincide for these cases. The amplification of acoustic pressure along the centerline is controlled by redistribution of the potential and kinetic parts of acoustic energy in this direction as opposed to the angular redistribution of acoustic energy (see the previous section). As far as the centerline profiles of the mean velocity and pressure are the same in Cases 3-A and 3-B, the profiles of acoustic pressure appear to be the same along the centerline. Note that this is quite a special situation where both the initial conditions of pulse and the background flow velocity are the same along the streamline for two different flows.

The maximum acoustic pressure for the transmitted wave is two times larger in Cases 3-A and 3-B than that in the Case 3-C. The maximum acoustic pressure for the reflected wave becomes about three times larger in presence of stagnation flow than that for the static ambient conditions.

The amplification of sound in the 3-D case is larger than that in the 2-D case. Recall that in both cases the background flow velocity and pressure are the same along the centerline. To get qualitative explanation of such a difference, the analytic solutions for acoustic pressure at the centerline (static ambient conditions) is presented for the 2-D and 3-D cases in Fig. 11a. The spatial derivative of acoustic pressure along the centerline is shown in Fig. 11b. By inspection of Fig. 11a and by comparison of derivatives in Fig. 11b, one can conclude that the back and front wave fronts are sharper in the 3-D case than those in the 2-D case. The front of the wave propagating upstream move slower than the back of it, that leads to the amplification of sound (see the previous section). The sharper the wave front is, the more prominent is the phenomenon. Therefore, the 3-D pulse in a 3-D stagnation flow amplifies larger than that in the 2-D case.

4. Aeroacoustics of the flow over a circular cylinder. The propagation of sound waves from a single acoustic pulse in the 2-D, inviscid irrotational, incompressible mean flow over an infinite circular cylinder is considered here. The computational domain is shown in Fig. 12. The circle of unit diameter ($R_{cyl} = 0.5$) is the inner boundary and a circle of 3.5 diameter is the outer boundary. At the outer boundary the mean flow is practically uniform. The streamlines of the mean flow and the isobars of mean pressure are computed analytically for potential flow [1] and presented in Fig. 12. The pulse is located at the centerline, in some distance from the rigid cylinder. While the mean flow is directed from left to right, the acoustic

waves, originated from the pulse, propagate upstream of the mean flow. Otherwise, the acoustic waves propagate downstream of the mean flow. The mean flow in front of the cylinder can be described by the incompressible potential flow model fairly well up to $M = 0.5$. The after-body flow can be described by this model when $M \leq 0.4$. It has been shown that the flow streamlines around cylinder are quite similar to those for incompressible flow if $M \leq 0.4$. [14]. For higher Mach number, strong recirculating zones appear at the rear part of the cylinder and the shock waves take place at the mid-section of the cylinder.

In polar (r, θ) coordinates, the equations of propagation of small disturbances in a known potential flow are given by

$$\frac{\partial u}{\partial t} = -\frac{\partial p}{\partial r} - U\frac{\partial u}{\partial r} - \frac{\partial U}{\partial r}u - U\frac{\partial U}{\partial r}\rho - \frac{1}{r}(V\frac{\partial u}{\partial \theta} + \frac{\partial U}{\partial \theta}v + V\frac{\partial U}{\partial \theta}\rho) - \frac{1}{r}\rho(V^2 - 2Vv)$$

$$\frac{\partial v}{\partial t} = -\frac{1}{r}\frac{\partial p}{\partial \theta} - \frac{1}{r}V\frac{\partial v}{\partial \theta} - U\frac{\partial v}{\partial r} - \frac{\partial V}{\partial r}u - U\frac{\partial V}{\partial r}\rho - \frac{1}{r}(\frac{\partial V}{\partial \theta}v + V\frac{\partial V}{\partial \theta}\rho) - \frac{1}{r}(\rho UV + Uv + Vu),$$

$$\frac{\partial \rho}{\partial t} = -\frac{\partial u}{\partial r} - U\frac{\partial \rho}{\partial r} - \frac{u}{r} - \frac{\rho U}{r} - \frac{1}{r}(\frac{\partial v}{\partial \theta} + V\frac{\partial \rho}{\partial \theta}), \tag{4.1}$$

where U, V, u, and v are radial and angular components of the mean flow velocity and disturbance velocity, respectively. The mean flow velocity and its derivatives are computed by [1]. The initial acoustic pulse is given by (2.9). The uniform grid 360×360 in polar computational space is used.

In Fig. 13, isobars of acoustic pressure at $t = 0.5$ are presented for upstream propagation of acoustic pulse (Case CYL-A) at $M = 0.5$, downstream propagation of acoustic pulse (Case CYL-B) at $M = 0.4$, and static ambient conditions (Case CYL-C). In Fig. 14, the centerline pressure distribution is presented for these cases at time moments $t = 0.5, 1.0, 1.5, 2$. In comparison with the Case CYL-C, the acoustic pressure is amplified at the neighborhood of the centerline in the Case CYL-A and is weakened in the Case CYL-B.

To get the sound directivity at different Mach numbers for Cases CYL-A and CYL-B, the root mean square of acoustic pressure is calculated by

$$p_{rms} = \sqrt{\int_0^T p^2 dt / T}, \tag{4.2}$$

where p is the acoustic pressure (p is equal to ρ) and T is the time period of summation. This time period is chosen constant and equal for all numerical experiments presented below. For temporal numerical integration, the integral in (4.2) is computed as sum of values of squares of acoustic pressure at all time steps over the period, T. The p^2 as a function of time for Cases CYL-A, CYL-B, and CYL-C at the centerline location $-5R_{cyl}$ is presented in Fig. 15. Curves have two stairs corresponding to passing transmitted and reflected waves. The time period, T, covers the pass of both waves. The p_{rms} represents the time-averaged potential part of acoustic energy passing through a fixed point in space.

In Fig. 16, the p_{rms} is shown as function of angle α from the centerline while the radial coordinate is equal to $-5R_{cyl}$. The curves are presented for various Mach numbers from $M = -0.4$ to $M = 0.5$ with step 0.1. The pressure pulse is located at the distance $0.25R_{cyl}$ from the cylinder (Fig. 16a,b) and at the distance $0.5R_{cyl}$ (Fig. 16c,d) at $t = 0$. The positive Mach numbers correspond to the Case CYL-A (Fig. 16a,c), the negative Mach numbers represent the Case CYL-B (Fig. 16b,d), and the zero Mach number is the Case CYL-C. The latter case is presented in (Fig. 16a-d) as a benchmark for comparison. The presented results are normalized in such a way that the p_{rms} at the centerline in the Case CYL-C is equal to unity.

The p_{rms} increases with the Mach number and reaches 2.2 while $M = 0.5$ (Fig. 16a). Even far apart from the centerline ($\alpha = 60°$), the p_{rms} for $M = 0.5$ is about twice as many as that for the Case CYL-C ($M = 0$) in the same direction.

For the Case CYL-B, the p_{rms} reduces with the absolute value of the Mach number and becomes 0.65 at the centerline while $M = -0.4$. The level of p_{rms} is smaller than that for the Case CYL-C up to $\alpha = 45^o$.

The degree of increase and reduction of acoustic pressure is slightly bigger when the pulse is located more close to wall (compare Fig. 16a,b with Fig. 16b,d). Note, that the difference between acoustic pressures is quite small for these pulse locations in Case CYL-C. The reason for such a difference for non-zero Mach numbers is that the reflected wave propagates in the direction opposite to the far-field sound before it hits the wall. For instance, in the Case CYL-A the reflected wave propagates downstream before its reflection from the cylinder and its acoustic pressure decreases.

5. Conclusions. The behavior of acoustic waves originating from the single pulse and propagated in the non-uniform incompressible background flow is studied by numerical simulation using Hardin and Pope approach. Higher-order compact spatial finite differences and Runge-Kutta temporal integration are used. Results are compared to those obtained for the same geometry in the static ambient conditions.

It is shown, that the acoustic pressure is almost doubled while the waves propagate upstream of the stagnation flow and the background flow reaches $M = 0.5$. Alternation of the direction of stagnation flow change the direction of sound propagation from perpendicular to a wall to parallel to it. Sound propagation in a corner while in the presence of the background inviscid flow leads to amplification of sound and flattening of acoustic waves.

In terms of acoustic energy, the modified sound directivity in the presence of stagnation flow is mainly caused by redistribution of potential and kinetic components of acoustic energy (while sound propagates upstream) and by angular redistribution of acoustic energy (while directions of the mean flow and sound propagation are far from collinear). The pump of acoustic energy from the background flow by means of baroclinically generated vorticity is minor.

The propagation of acoustic wave originated from spherical pulse in 3-D stagnation flows was considered and the wave pattern in the neighborhood of the single stagnation point and the stagnation line are discussed. The amplification of sound by a mean flow is more prominent in the 3-D case than in the 2-D case because of steeper acoustic wave bounds.

Finally, the propagation of acoustic pulse in the flow around the 2-D circular cylinder is modeled. The time-averaged root mean square of acoustic pressure (rms) is presented as function of angle from the centerline. To compare with the static ambient conditions, the rms of acoustic pressure at the centerline is approximately doubled (upstream pulse position, $M = 0.5$) and halved (downstream pulse position, $M = 0.4$). The amplification (upstream pulse position) and weakening (downstream pulse position) of sound holds for a large angular sector apart from the centerline.

This study can be expanded to cases where a compressible mean flow is computed by a CFD method and the acoustic source distribution is extracted from appropriate turbulence modeling. Investigation of sound amplification is expected to be important for higher Mach number flows where the velocity and pressure gradients in the mean flow are larger than those in the low-Mach-number flows considered here.

<div align="center">REFERENCES</div>

[1] J. ANDERSON, *Fundamentals of Aerodynamics*, McGraw-Hill, New York, 1984.
[2] H. ATASSI AND J. GRZEDZINSKI, *Unsteady Disturbances of Streaming Motions Around Bodies*, J. Fluid Mech., 209 (1989), pp. 385–403.
[3] G. K. BATCHELOR, *An Introduction to Fluid Mechanics*, Cambridge University Press, London, 1974.

[4] M. H. CARPENTER, D. GOTTLIEB, AND S. ABARBANEL, *The Stability of Numerical Boundary Treatments of Compact High-order Finite-difference Schemes*, J. Comput. Phys., 108 (1993), p. 272.

[5] M. GOLDSTEIN, *Aeroacoustics*, McGraw-Hill, New York, 1976.

[6] J. HARDIN AND D. S. POPE, *A New Technique for Aerodynamic Noise Calculation*, in Proceedings of the DGLRR/AIAA 14th Aeroacoustics Conference, Washington, DC, 1992, pp. 448–456.

[7] J. C. HARDIN, J. R. RISTORCELLI, AND C. K. W. TAM, *ICASE/LaRC Workshop on Benchmark Problems in Computational Aeroacoustics*, Hampton, VA, 1995.

[8] C. HIRSCH, *Numerical Computation of Internal and External Flows, Vol. 1: Fundamentals of Numerical Discretizations*, John Wiley, Chichester, 1994.

[9] S. K. LELE, *Compact Finite Difference Schemes with Spectral Like Resolution*, J. Comput. Phys., 103 (1992), pp. 16–42.

[10] A. NAYFEH, J. KAISER, AND B. SHAKER, *Transmission of Sound through Nonuniform Circular Ducts with Compressible Mean Flows*, AIAA Journal, 18 (1980), pp. 515–525.

[11] A. POVITSKY, *On aeroacoustics of a stagnation flow near a rigid wall*, Physics of Fluids, (October 2000, to appear). Preprint: ICASE Report No. 99-48.

[12] A. POVITSKY AND P. MORRIS, *A parallel compact multi-dimensional numerical algorithm with aeroacoustics applications*, Journal of Computational Physics, 161 (2000), pp. 182–203. Preprint: ICASE Report No. 99-34.

[13] M. SALAS, *Recent Developments In Transonic Euler Flow Over a Circular Cylinder*, Mathematics and Computers in Simulation, 25 (1982), pp. 232–236. NASA TM 83282, 1982; the paper presented at the 10th IMACS World Congress, Montreal, Canada, Aug. 8-13, 1982.

[14] K. UENISHI AND M. MYERS, *Two-Dimensional Acoustic Field in a Nonuniform Duct Carrying Compressible Flow*, AIAA Journal, 22 (1984), pp. 1242–1248.

[15] J. WILLIAMSON, *Low Storage Runge-Kutta Schemes*, J. Comput. Phys., 35 (1980), pp. 48–56.

[16] R. V. WILSON, A. O. DEMUREN, AND M. CARPENTER, *High-Order Compact Schemes for Numerical Simulation of Incompressible Flows*, ICASE Report No. 98-13, 1998.

[17] S. WOLFRAM, *The Mathematica book*, Cambridge University Press, Third Edition, 1996.

Appendix A. Mean-flow variables for a flow between two straight streamlines.

In Cartesian coordinates, the stream-function is given by

$$\psi = A(x^2 + y^2)^{0.5n} sin(n \arctan(x/y)), \tag{A.1}$$

The velocity field $(U(x,y), V(x,y))$ is computed by differentiation of the stream-function defined above

$$U(x,y) = \frac{\partial \psi}{\partial y}, \ \ V(x,y) = -\frac{\partial \psi}{\partial x} \tag{A.2}$$

Using *Mathematica* [18], the following expressions for velocities and their derivatives are obtained

$$U(x,y) = Anr^{n-2}(x \cos n\theta + y \sin n\theta), \tag{A.3}$$

$$V(x,y) = Anr^{n-2}(y \cos n\theta - x \sin n\theta), \tag{A.4}$$

$$\frac{\partial U(x,y)}{\partial x} = Anr^{n-4}((n-1)(y^2 - x^2) \cos n\theta + 2(n-1)xy \sin n\theta), \tag{A.5}$$

$$\frac{\partial U(x,y)}{\partial y} = Anr^{n-4}((n-1)(x^2 - y^2) \sin n\theta - 2(n-1)xy \cos n\theta), \tag{A.6}$$

where $r = \sqrt{(x^2 + y^2)}$, and $\theta = \arctan(x/y)$.

For an incompressible and irrotational mean flow,

$$\frac{\partial U(x,y)}{\partial x} = -\frac{\partial V(x,y)}{\partial y}, \ \ \frac{\partial U(x,y)}{\partial y} = \frac{\partial V(x,y)}{\partial x}. \tag{A.7}$$

Level p
15   1.9277E-03
14   1.7232E-03
13   1.5187E-03
12   1.3141E-03
11   1.1096E-03
10   9.0508E-04
9   7.0055E-04
8   4.9602E-04
7   2.9149E-04
6   8.6965E-05
5   -1.1756E-04
4   -3.2209E-04
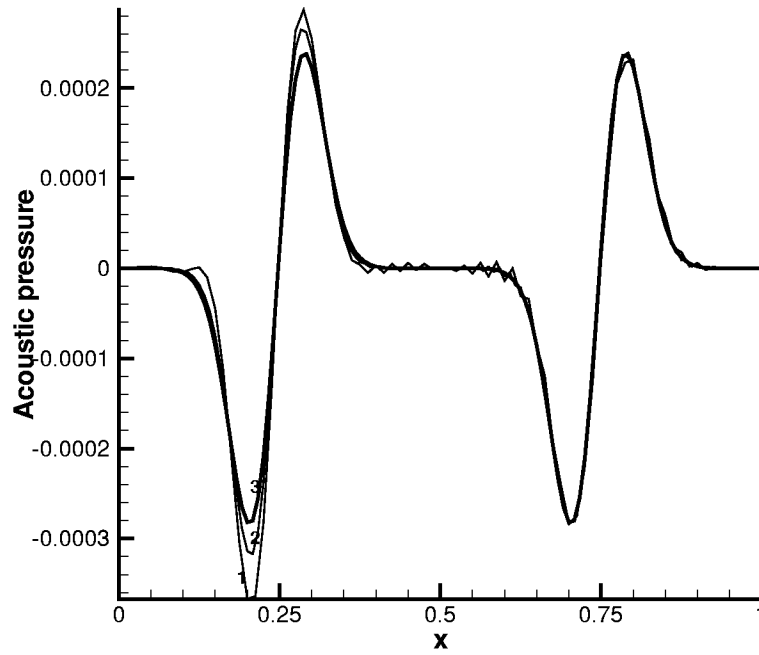3   -5.2662E-04
2   -7.3114E-04
1   -9.3567E-04
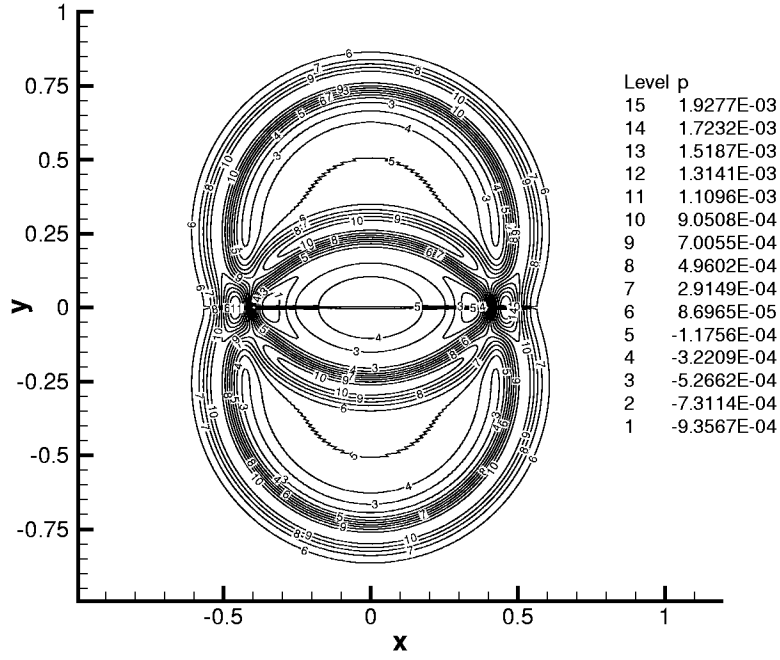
a.
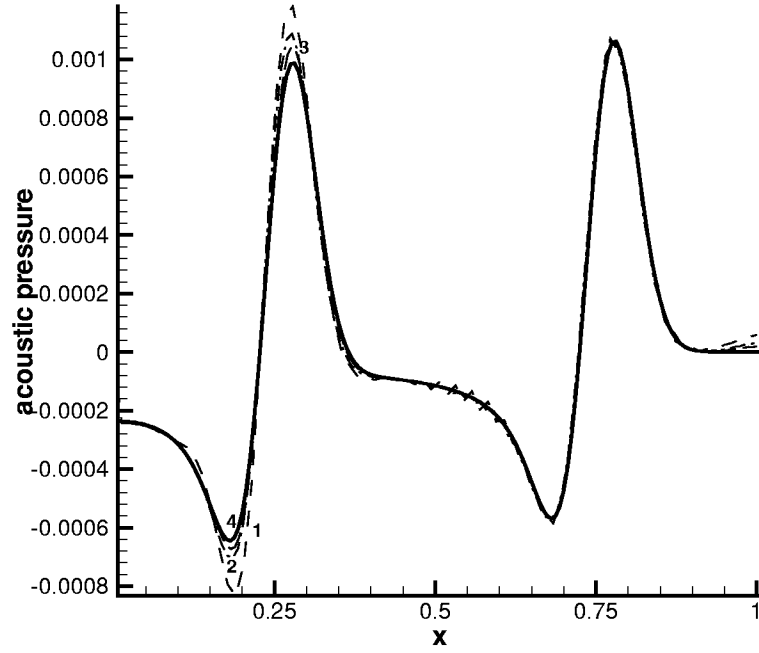
b.

FIG. 1. *Acoustic pulse propagation in the static ambient conditions in presence of the rigid wall. a) Isolines of acoustic pressure. Combined computational domain* $[-1,1] \times [-1,1]$; *is covered with the* 320×320 *grid. b) Profiles of the centerline acoustic pressure. Computational domain* $[-1,1] \times [0,1]$ *is covered with the following numerical grids 1)* 80×80; *2)* 120×120; *and 3)* 160×160; *4) is the analytical solution [8].*
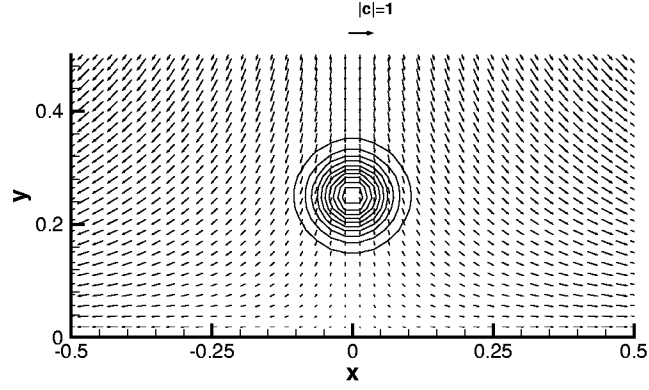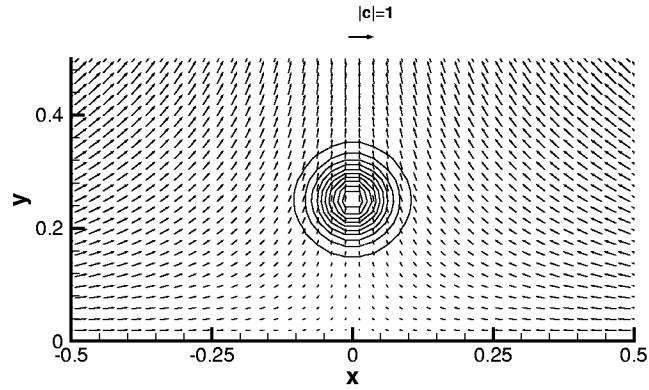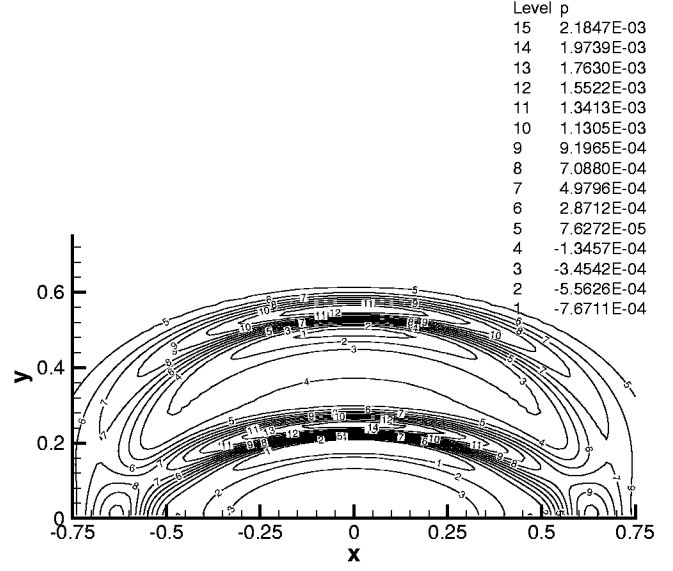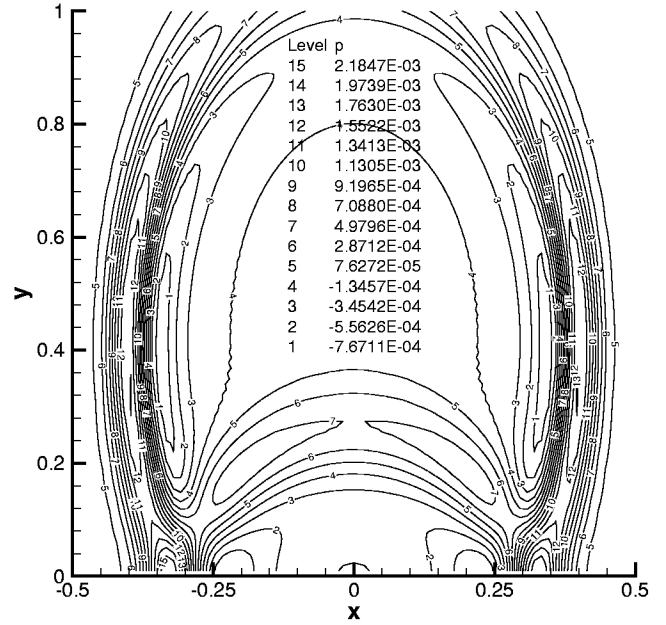
FIG. 2. *Acoustic pulse propagation in the 2-D stagnation flow: a) forward stagnation flow, $A = -0.5$, and b) backward stagnation flow, $A = 0.5$, Eq. (2.1). The left column shown the mean flow and the isobars of acoustic pulse at $t = 0$, the right column presents acoustic isobars.*

14

a.

b.

c.
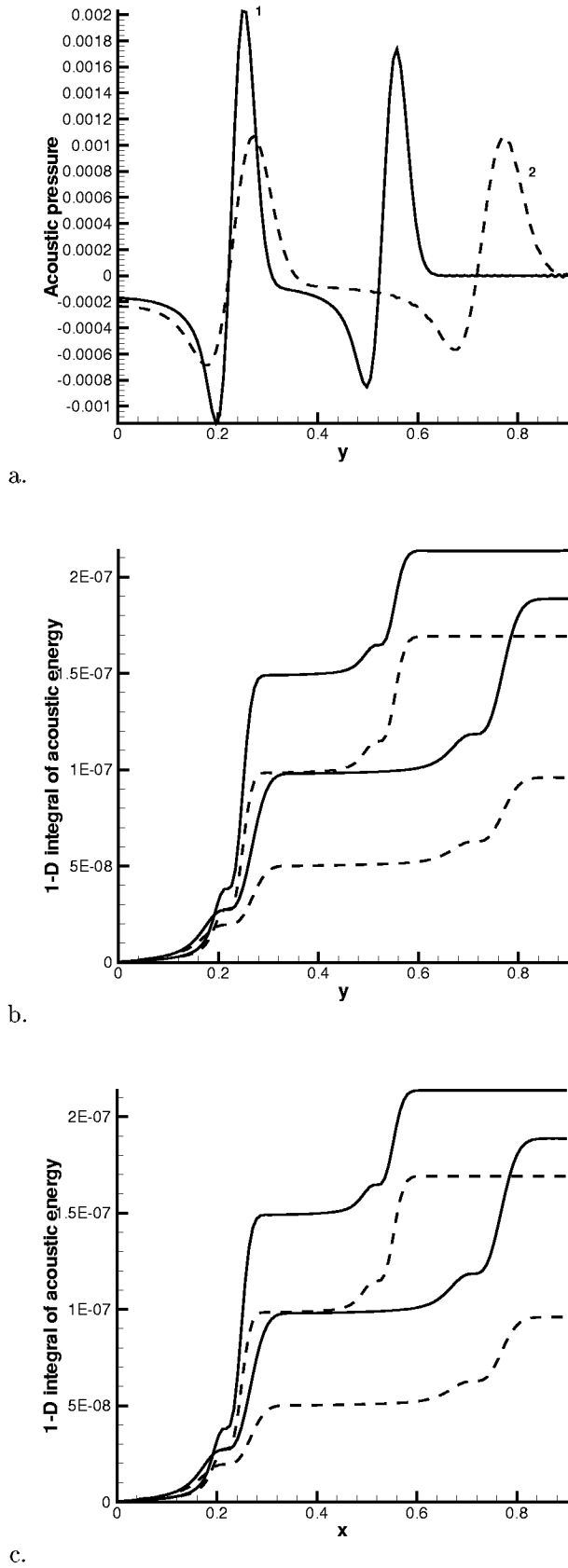
FIG. 3. *Acoustic pressure, acoustic energy (2.10), and integral of acoustic energy (2.13 and 2.14) along the centerline. Here (1) is the Case 2-A and (2)-is the Case 2-B. In graph (c), solid lines denote integral of acoustic energy (2.13), and dashed lines denote integral of potential part of acoustic energy (2.14)*
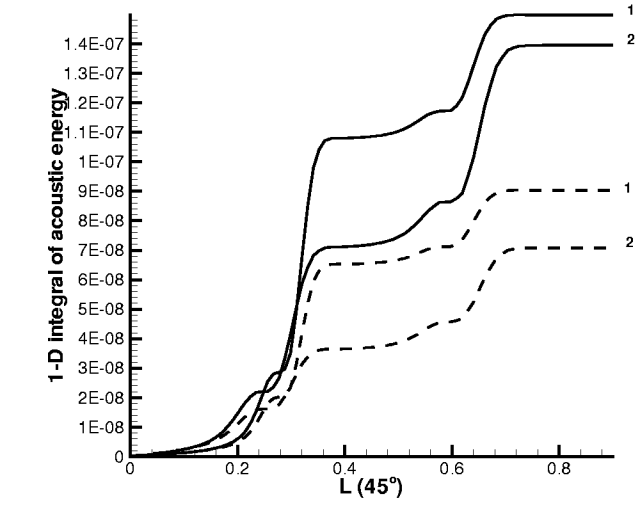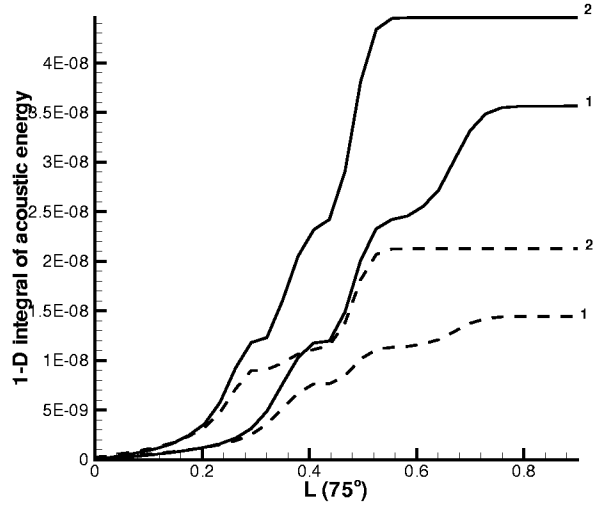
FIG. 4. *Integral of acoustic energy and its potential part in various spatial directions: a) 45°, and b) 75°. The legend is the same as for the previous figure.*

13	6.4678E-03
11	4.4777E-03
9	2.4876E-03
7	-1.4925E-03
5	-3.4826E-03
3	-5.4727E-03
1	-7.4628E-03

15	1.6960E-07
13	1.4664E-07
11	1.2369E-07
9	1.0074E-07
7	7.7786E-08
5	5.4834E-08
3	3.1882E-08
1	8.9292E-09

a.   b.
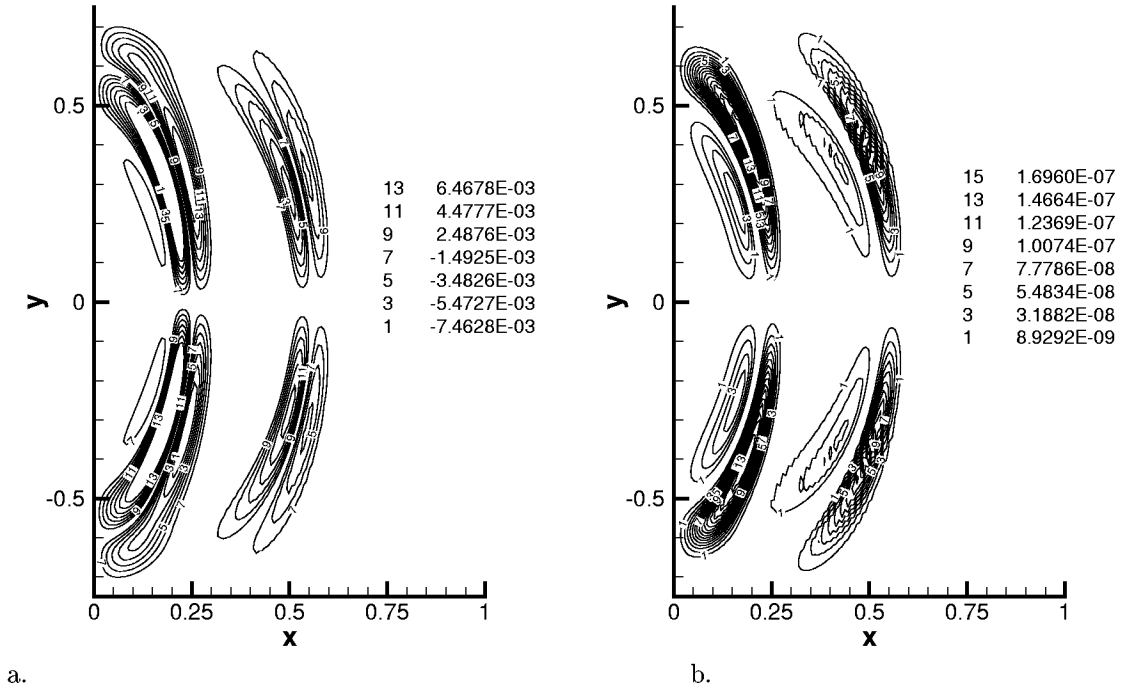
FIG. 5. *Generation of acoustic energy (Case 2-A): a) generation of vorticity, and b) generation of acoustic energy.*
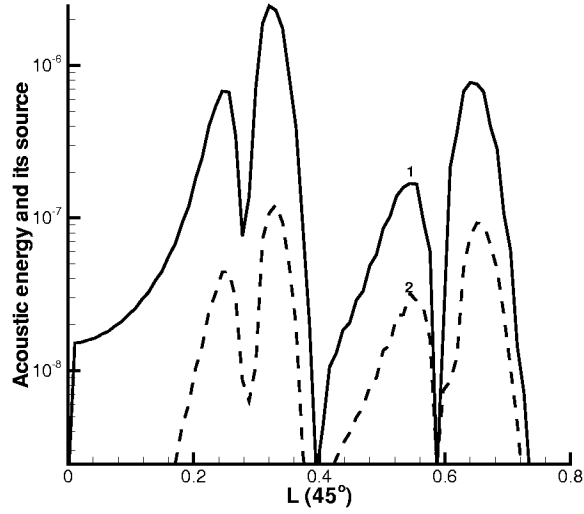
FIG. 6. *Acoustic energy and its source along the bisector $\alpha = 45^o$ at $t = 0.5$, where 1) is the acoustic energy (solid line), and 2) is the source of energy (dashed line). $L(45^o)$ is the distance from the origin along the bisector*

17
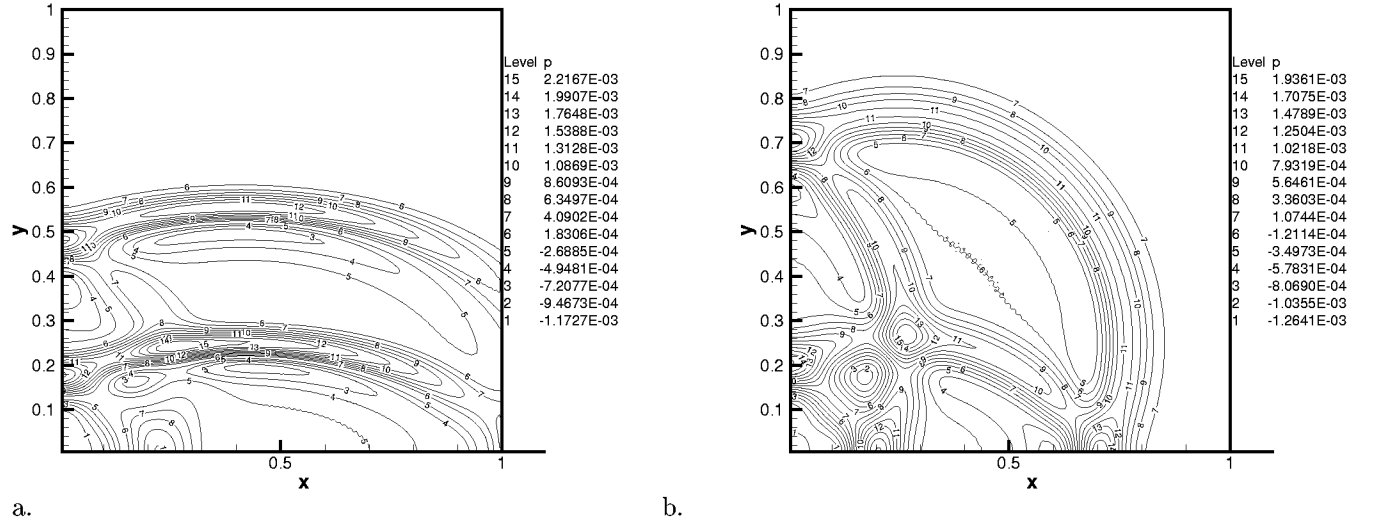
FIG. 7. *Acoustic pulse propagation in a* 90^0 *corner at* $t = 0.5$: *a) in presence of the inviscid flow, and b) in the static ambient conditions.*

FIG. 8. *3-D acoustic pulse propagation in the static ambient conditions in presence of rigid wall. Computational domain:* $[-1, 1] \times [-1, 1] \times [0, 1]$ *1)* 80×80; *2)* 120×120; *and 3) analytical solution.*
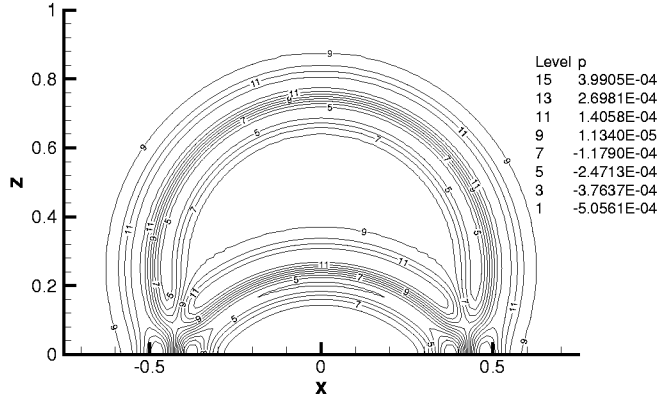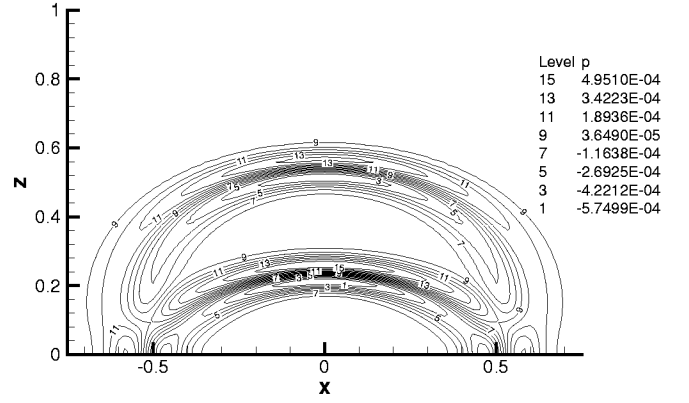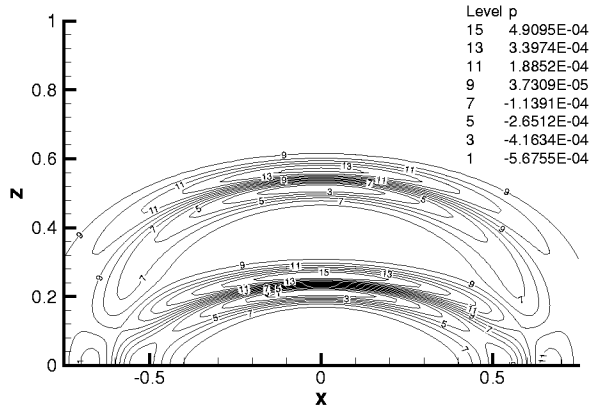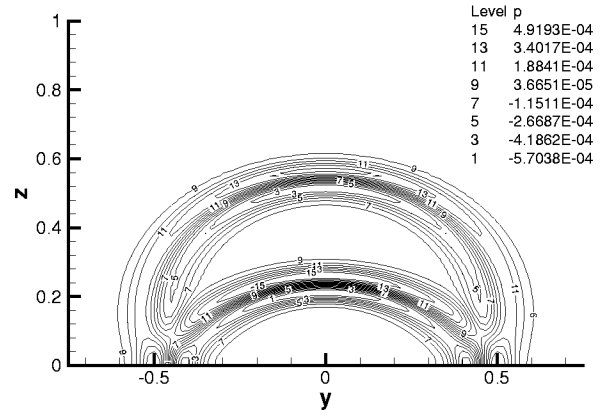
FIG. 9. *Isobars of acoustic pressure for 3-D pulse at* $t = 0.5$: *a) static ambient conditions, b) stagnation mean flow (3.1) c-d) stagnation flow (3.2), where c)* $x - z$ *section, d)* $y - z$ *section.*
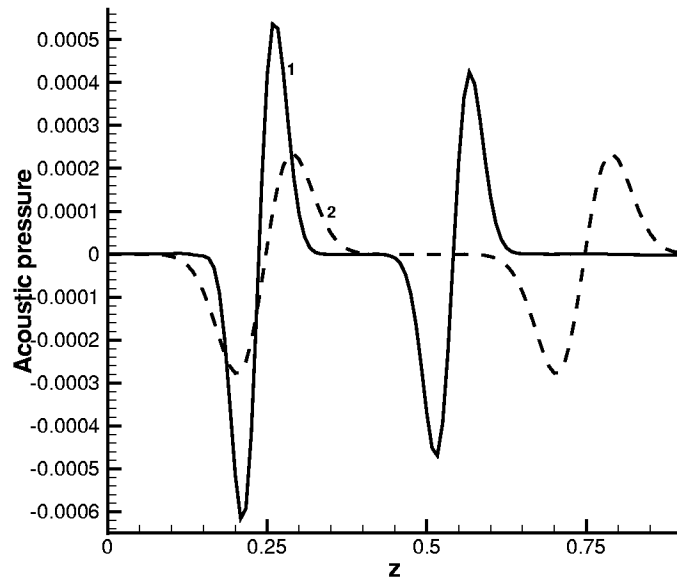
FIG. 10. *Axial profile of acoustic pressure: (1)-stagnation mean flows (3.1) and (3.2) (Cases 3-A and 3-B), and (2) static ambient conditions (Case 3-C).*
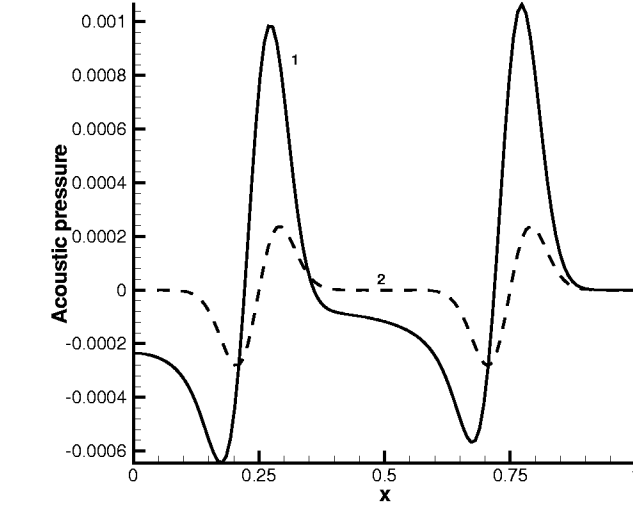
a.
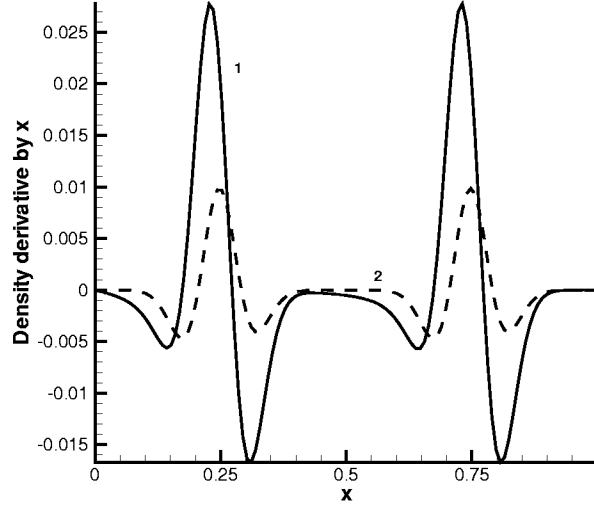
b.

FIG. 11. *Acoustic pulse propagation and reflection in static ambient conditions (analytic solution): a) centerline acoustic pressure, b) the spatial derivative of acoustic pressure along the centerline. The direction of the x−coordinate coincides with the centerline, graphs (1) and (2) denote 2-D cylindrical pulse (Case 2-B) and 3-D spherical pulse (Case 3-C), respectively.*
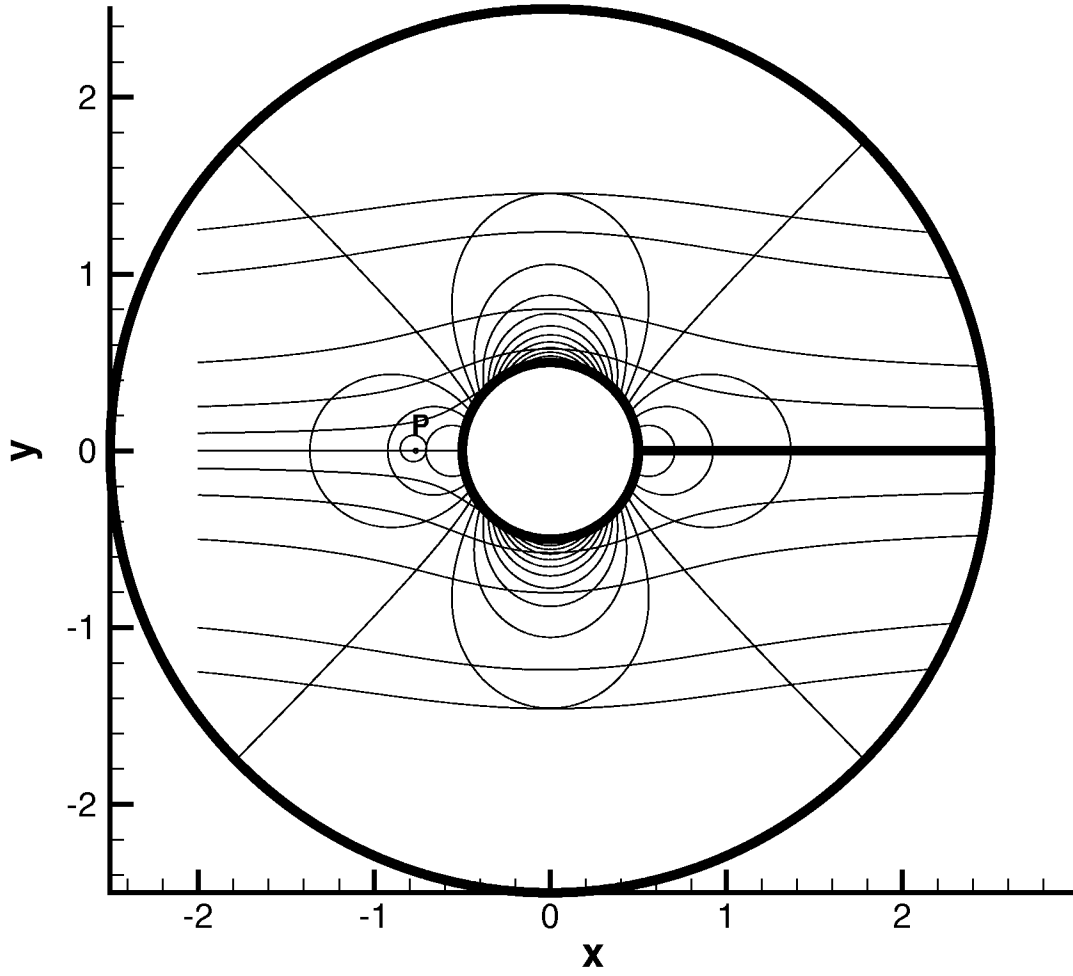
FIG. 12. *Potential non-lifting flow over a circular cylinder. Here P denote initial position of acoustic pulse, and thick lines denote boundaries of cylindrical computational domain. Isolines of mean pressure and streamlines are shown.*
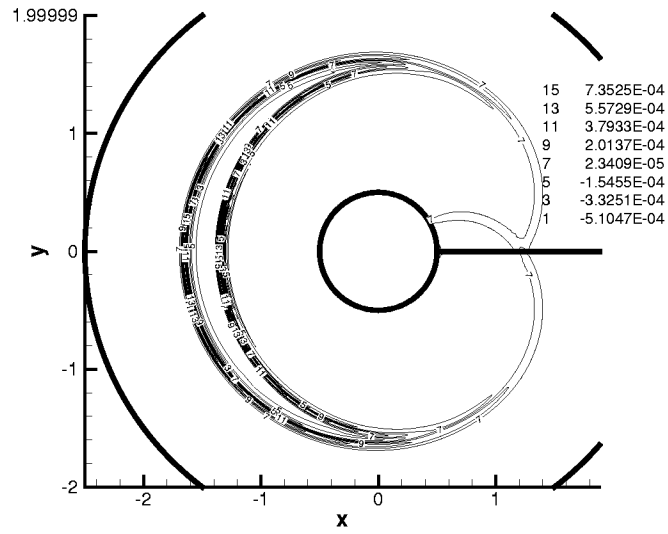
a
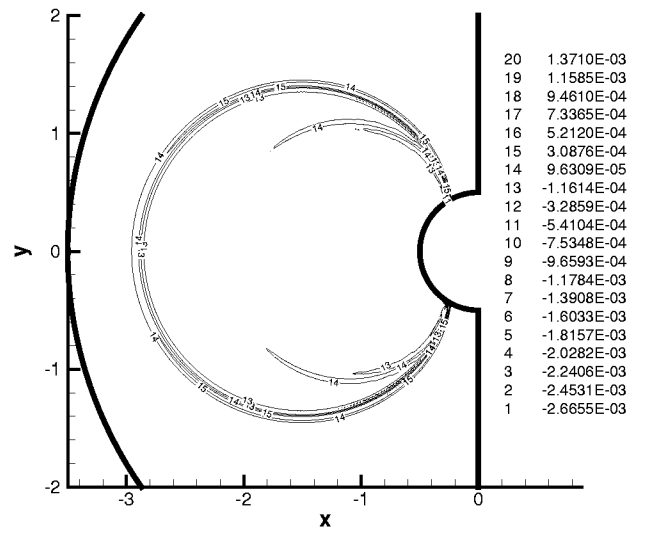
b
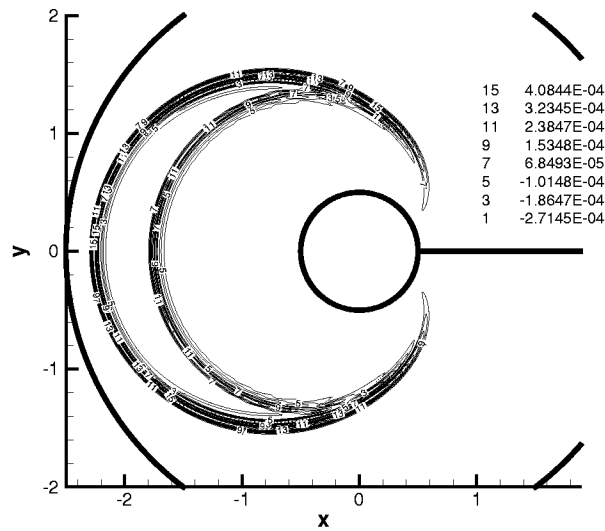
c.

FIG. 13. *Isobars of acoustic pressure at* $t = 1.5$. *a) upstream propagation of sound (Case CYL-A) b) downstream propagation of sound (Case CYL-B), and c) static ambient conditions (Case CYL-C). The direction of* $x-$ *coordinate coincides with the centerline. Time moments: 1)* $t = 0.5$; *2)* $t = 1.0$; *3)* $t = 1.5$; *4)* $t = 2.0$.

23
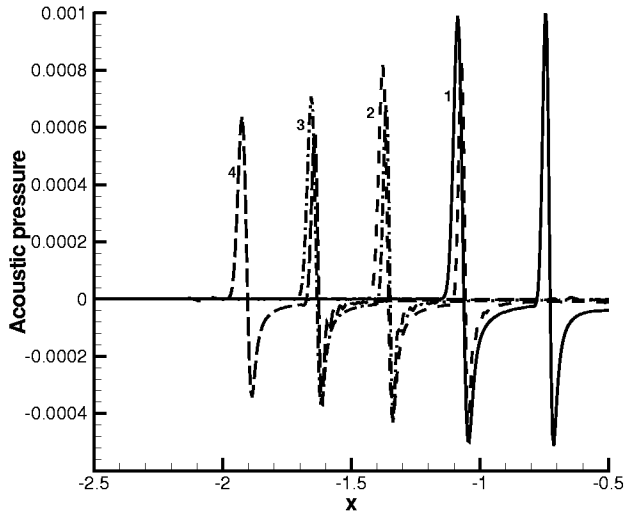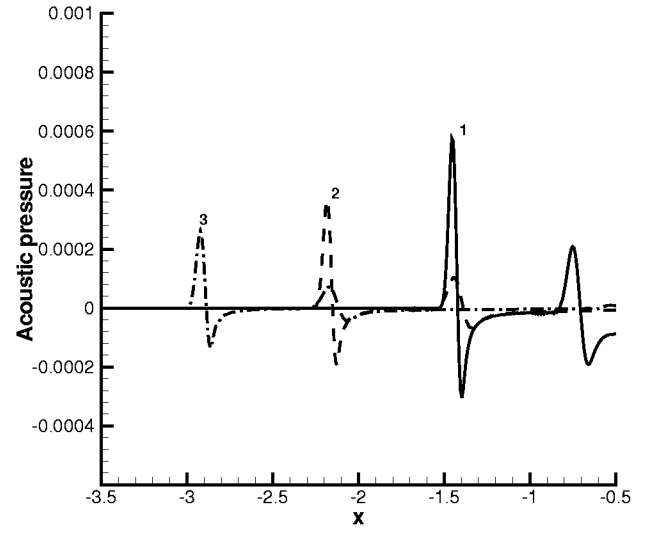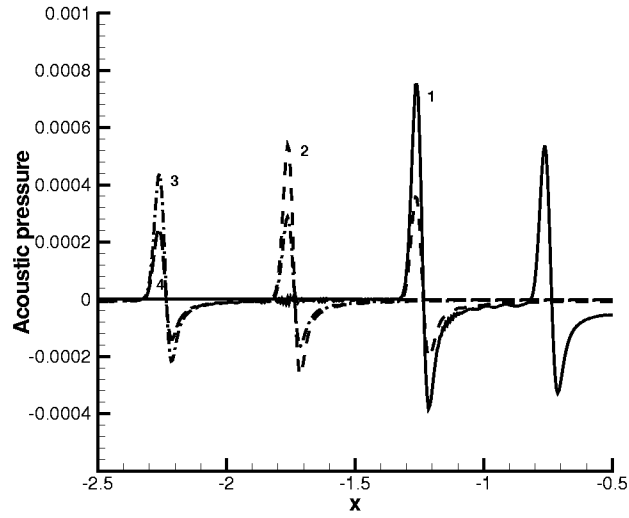
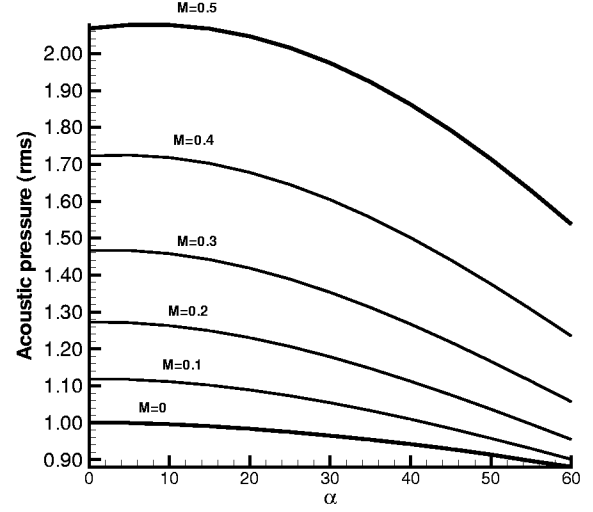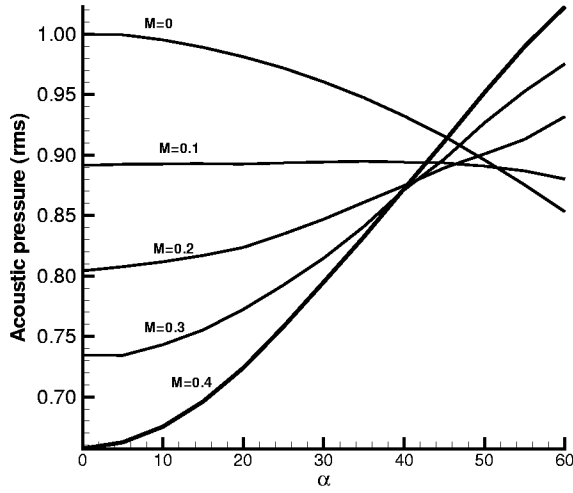FIG. 14. *Centerline acoustic pressure for pulse near a circular cylinder: Conditions for graphs (a-c) are the same as in the previous figure.*
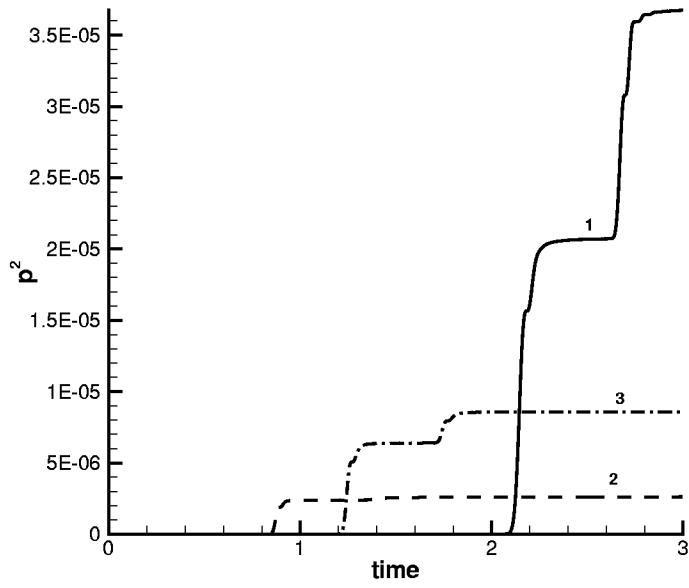
FIG. 15. *Square of acoustic pressure. Here (1) is the Case CYL-A ($M = 0.5$), (2) is the Case CYL-B ($M = 0.4$), and (3) is the Case CYL-C. Observer is located at the centerline at the distance $5R_{cyl}$ from the origin.*
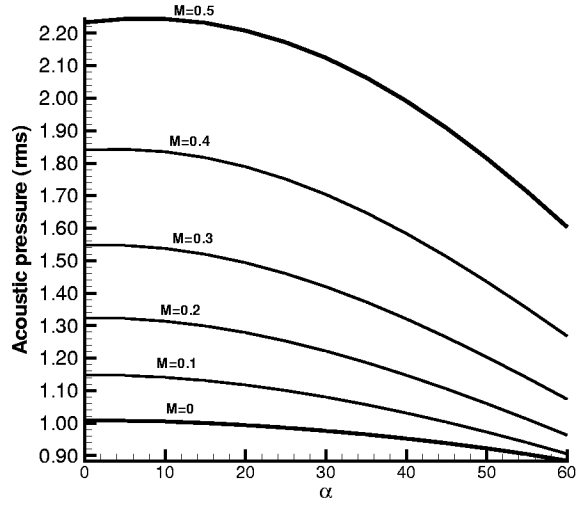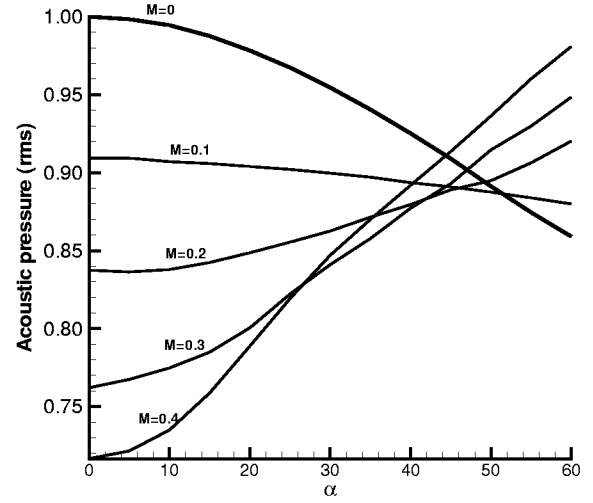
FIG. 16. *Root mean square (rms) of acoustic pressure: a,b) pulse location* $R_{init} = 0.25 R_{cyl}$, *c,d) pulse location* $R_{init} = 0.5 R_{cyl}$, *a,c) upstream propagation (Case CYL-A), b,d) downstream propagation (Case CYL-B)*

REPORT DOCUMENTATION PAGE

1. AGENCY USE ONLY *(Leave blank)*	2. REPORT DATE September 2000	3. REPORT TYPE AND DATES COVERED Contractor Report

4. TITLE AND SUBTITLE
Numerical study of wave propagation in a non-uniform flow

5. FUNDING NUMBERS
C NAS1-97046
WU 505-90-52-01

6. AUTHOR(S)
Alex Povitsky

7. PERFORMING ORGANIZATION NAME(S) AND ADDRESS(ES)
Institute for Computer Applications in Science and Engineering
Mail Stop 132C, NASA Langley Research Center
Hampton, VA 23681-2199

8. PERFORMING ORGANIZATION REPORT NUMBER
ICASE Report No. 2000-35

9. SPONSORING/MONITORING AGENCY NAME(S) AND ADDRESS(ES)
National Aeronautics and Space Administration
Langley Research Center
Hampton, VA 23681-2199

10. SPONSORING/MONITORING AGENCY REPORT NUMBER
NASA/CR-2000-210533
ICASE Report No. 2000-35

11. SUPPLEMENTARY NOTES
Langley Technical Monitor: Dennis M. Bushnell
Final Report
To be submitted to the Journal of Computational Physics.

12a. DISTRIBUTION/AVAILABILITY STATEMENT
Unclassified–Unlimited
Subject Category 34
Distribution: Nonstandard
Availability: NASA-CASI (301) 621-0390

12b. DISTRIBUTION CODE

13. ABSTRACT *(Maximum 200 words)*
The propagation of acoustic waves originating from cylindrical and spherical pulses, in a non-uniform mean flow, and in the presence of a reflecting wall is investigated by Hardin and Pope approach using compact approximation of spatial derivatives. The 2-D and 3-D stagnation flows and a flow around a cylinder are taken as prototypes of real world flows with strong gradients of mean pressure and velocity. The intensity and directivity of acoustic wave patterns appear to be quite different from the benchmark solutions obtained in a static environment for the same geometry. The physical reasons for amplification and weakening of sound are discussed in terms of dynamics of wave profile and redistribution of acoustic energy and its potential and kinetic components. For an acoustic wave in the flow around a cylinder, the observed mean acoustic pressure is approximately doubled (upstream pulse position) and halved (downstream pulse position) in comparison with the sound propagation in static ambient conditions.

14. SUBJECT TERMS
aeroacoustics, non-uniform mean flow, higher-order compact scheme, amplification of sound, stagnation flow, flow around cylinder

15. NUMBER OF PAGES
31

16. PRICE CODE
A03

17. SECURITY CLASSIFICATION OF REPORT Unclassified	18. SECURITY CLASSIFICATION OF THIS PAGE Unclassified	19. SECURITY CLASSIFICATION OF ABSTRACT	20. LIMITATION OF ABSTRACT